Mine waste from carbonatite deposits as potential rare earth resource: insight into Phalaborwa (Palabora) Complex

Alba Gómez-Arias[1,2,3], Lola Yesares[4,5], Joaquín Díaz[2], Manuel A. Caraballo[6,7,8,9], Maleke Maleke[10], Reinaldo Sáez[2], Esta van Heerden[11], Danie Vermeulen[1], José M. Nieto[2], Julio Castillo[3*]

[1]*Institutite for Groundwater Studies, University of the Free State, Nelson Mandela Drive, 9301 Bloemfontein, Republic of South Africa.*

[2]*Department of Earth Sciences & Research Center on Natural Resources, Health and the Environment, University of Huelva, Campus 'El Carmen', 21071 Huelva, Spain.*

[3]*Department of Microbiology and Biochemistry, University of the Free State,9301 Bloemfontein, Republic of South Africa.*

[4]*iCRAG and School of Earth Sciences, University College Dublin, Beldfield 4, Ireland.*

[5]*Mineralogy and Petrology Department, Complutense University of Madrid, Av. Complutense s/n, 28040 Madrid, Spain*

[6] *Advanced Mining Technology Center, University of Chile, Avda. Tupper 2007, 8370451 Santiago, Chile*

[7]*Mining Engineering Department, University of Chile, Avda. Tupper 2069, Santiago, Chile.*

[8]*Department of Water, Mining and Environment, Scientific and Technological Center of Huelva, University of Huelva, 21004 Huelva, Spain*

[9]*Department of Mining, Mechanic, Energetic and Construction Engineering, Higher Technical School of Engineering, University of Huelva, Avda. de las Fuerzas Armadas, S/N, 21071 Huelva, Spain*

[10]*Life Science, Central University of Technology, 9301 Bloemfontein, Republic of South Africa*

[11]*iWater, North West University, 5 Walter Sisulu Rd, Park West, 9301 Bloemfontein, Republic of South Africa*

**Corresponding author: Julio Castillo, ORCID: 0000-00027-9070-882 phone: +27794581857, email: castillohernandezj@ufs.ac.za*

Abstract

Phalaborwa (Palabora) Igneous Complex (PIC), South Africa, has been mined for the last six decades for copper and phosphate, among others commodities. As a result, more than 4,500 Mt of mining wastes have been dumped in waste rock dumps (WRDs) and tailing impoundments. This study aims to investigate the potential of the PIC wastes as a secondary resource of rare earth elements (REE) and its possible processing options, by means of both mineralogical and geochemical determinations. Phoscorites and carbonatites are major lithologies in the WRDs and contain a notable concentration of REE, of which 0.2 and 0.1 wt%, respectively, would be easily extractable. The mineralogical results show monazite as the main REE-mineral (∑REE 60 wt%), while fluorapatite and calcite are the most important REE-bearing minerals (∑REE 1 and 0.5 wt%, respectively) for their abundance. On the other hand, the tailings are comprised mostly by monomineralic particles of calcite, dolomite, pyroxene, fluorapatite, magnetite and phlogopite. Based on the geochemical results, the extraction of REE from monazite, fluorapatite, calcite and dolomite, from tailings produced by both the Cu and the phosphate mines, might produce up to 5.65 and 1.75 kg of REE per ton, respectively. Therefore, tailings from PIC have the potential to become an asset. An approach to circular

economy by re-processing mining wastes would extend the lifetime of PIC mines and their benefits, while reducing the waste of resources and their environmental impact.

Keywords: Tailings, waste rock dumps, rare earth elements, secondary resource, revalorization

1. Introduction

Rare Earth Elements (REE), including lanthanides, yttrium and scandium, can be subdivided into light REE (LREE) for La, Ce, Pr and Nd; medium REE (MREE) for Sm, Eu and Gd; and heavy REE (HREE) for Tb, Dy, Ho, Er, Tm Yb, Lu, Y and Sc. All of them are classified as critical raw materials (CRM) (EC-DG ENTR, 2014). Nassar et al. (2020) has shown how REE disruption potential (understood as a producing country's ability and willingness to supply the U.S.) has decreased in the past few years thanks to the increased production diversification, particularly outside of China. However, REE still pose the greatest supply risk for the manufacturing sector. Resulting from this recent economic and supply risk assessment, the ability to diversify the REE supply sources and include new alternative resources and strategies (e.g., mine wastes revalorization and reprocessing) are of paramount importance for both world´s economy and geopolitical stability.

REE crustal abundance typically range from 0.5 to 60 ppm, but minable deposits are scarce comprising only 120 Mt of the global reserves (Krishnamurthy and Gupta, 2015). Economic REE concentrations are mainly associated with carbonatites, peralkaline igneous deposits and REE-bearing clays and placer deposits (Gambogi, 2019). Carbonatites are the main source of light rare earth elements (LREE) and Sc. Currently, 527 carbonatite occurrences have been reported worldwide, of which 43 deposits have been found in South Africa (Madugalla et al., 2014; Owen and Madari, 2009; Verwoerd, 1993; Woolley, 2001). Among them, Phalaborwa Igneous Complex (PIC) is the most noticeable and unique economic carbonatitic-hosted Cu deposit on Earth (Hanekom et al., 1965). Previous petrogenetic studies of PIC have highlighted the occurrence of REE-minerals, particularly in fresh carbonatite and phoscorite rocks (Dawson and Hinton, 2003; Giebel et al., 2019, 2017; Milani et al., 2017).

Mine residues reprocessing is widely studied nowadays around the world. At PIC, the intense mining of Cu and phosphate generate about 18 and 29 Mt of waste per year, respectively (Foskor, 2018; Golder Associates, 2019). Part of it is reprocessed to extract magnetite, Zr, Ni and anode slimes with Au, Ag and Pt (Foskor, 2018; Valderrama et al., 2011; Zhang et al., 2014). However, no previous studies have addressed the potential revalorization of PIC's waste rock dumps (WRD) and tailings as secondary source of REE.

The present study encompasses a comprehensive mineralogical and geochemical characterization of REE content in PIC's tailings and WRDs, as well as envisages the first estimation for the revalorization and reclassification of these mining residues as a possible REE resource. In addition, the mineralogical characterization of REE occurrences in these residues could assist in future mineral processing in this industrial complex.

2. Site description

2.1. Geological setting

Phalaborwa (Palabora) Igneous Complex (PIC) is located in the North-Western edge of the Kaapvaal Craton, associated with a series of intrusions of Paleoproterozoic alkaline magmas (Aldous, 1986; Basson et al., 2017; Hanekom et al., 1965). This complex is a pipe-like intrusion with three well-differentiated sections (Figure 1); (1) the Northern Pyroxenite, formed mainly of olivine and phlogopite. It shows pegmatite-like textures and pervasive alteration to serpentine and vermiculite; (2) the Southern Pyroxenite comprised mostly by coarse grained phlogopite and vermiculite and subordinated apatite and pyroxene; and (3) the Central Carbonatite, also known as the Loolekop pipe, constitutes a concentric structure made of three ring–like bodies. From outside inwards, they are: i) the outermost pegmatitic-pyroxenite body, composed by pyroxene, phlogopite and fluorapatite; ii) the intermediate phoscorite, which is mainly formed by hydroxyapatite and fluorapatite, partially serpentinized olivine and magnetite; and iii) the carbonatite core mainly composed of carbonates (calcite and dolomite), fluorapatite, chondrodite, olivine, phlogopite and biotite. This carbonatite core includes two facies; the outer and older, banded carbonatite (B-carbonatite) and the inner and younger, transgressive carbonatite (T-carbonatite). The main phosphate ore is associated to the intermediate phoscorite whereas the Cu mineralization is linked to the carbonatitic core (Briden, 1976; Giebel et al., 2019, 2017; Hanekom et al., 1965; Heinrich, 1970; Stettler et al., 1989; Uken and Watkeys, 1997; Verwoerd, 1993; Wilkin and Barnes, 1997; Wu et al., 2011).

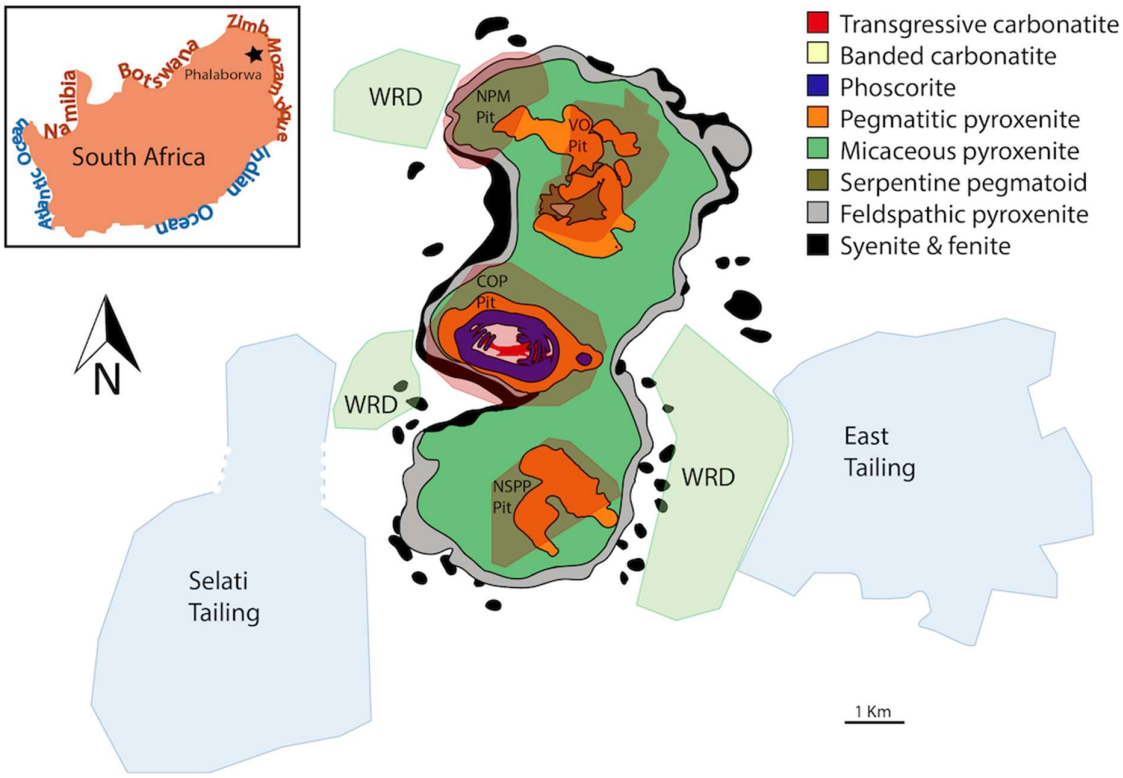

Figure 1. Simplified geological map of Phalaborwa Igneous Complex (modified from Giebel et al., 2019). Red shadows include the Cu open pit (COP), the North Pyroxenite Mine (NPM) pit, the New South Pyroxenite Pit (NSPP) and Vermiculite Open (VO) Pit; Blue shadows represent the East and Selati tailing dams; and shaded in green are represented the waste rock dumps (WRDs).

2.2. Location and industrial operations

The complex is located in the Limpopo province of South Africa, adjacent to the town of Phalaborwa and the Kruger National Park. The mining activities began in the 1950s with the extraction of phosphate and Cu minerals. Currently, 50 km^2 of the complex is occupied by a synergic network of mining companies dedicated mainly to the extraction of Cu, phosphate and vermiculite (Brink, 2011; Foskor, 2018; Steyl, 2011). Decades of mining activity in this area has generated multiple WRDs and tailings (Figure 1). The main WRD of PIC is located east of the Cu open pit (COP) (both decommissioned) and collected the removal of COP overburden. It has a height of 105 m above ground level and piles about 1,085 Mt of mainly barren carbonatites, and minor barren phoscorites and pyroxenites. Two smaller WRDs, located southwest (decommissioned) and northwest (active) of COP, collect mainly barren pyroxenites and phoscorites from North Pyroxenite Mine (NSPP), New South Pyroxenite Pit (NPM) and Vermiculite Open (VO) pit (Figure 1) (Brink, 2011; Moukodi, 2008). Selati tailing is located in the southern most area of PIC, intersected by the Ga-Selati River. This has been the largest tailing in the southern hemisphere, with about 2,830 Mt of processed material from

the phosphate plant (Foskor, 2018). The East tailing is located in the eastern most part of PIC, which collects about 575 Mt of the residues after carbonatite froth-flotation from the Cu beneficiation (Hu et al., 2017; Moukodi, 2008).

3. Samples and methods

3.1. Waste rock and tailing sampling

A set of 60 samples, ranging from 1 to 12 kg each, were collected from the PIC's WRDs, including all the representative lithological-type fragments. Tailing samples were collected from 6 different sectors. A composite of approximately 5 kg and up to 2m depth, were taken from each section (Figure 1), including six samples of recently piled tailings and 14 samples of different ages. The description and coordinates of the sampling points for both WRD and tailings are displayed in Appendix 1.

Rock samples were split, half-samples were crashed, milled, homogeneously mixed and representative subsamples were collected using a sampler splitter for sequential extraction assays. The remaining rocks were used for mineralogical characterization. Tailing samples were homogeneously mixed and split for further chemical and mineralogical analysis.

3.2. Mineralogical characterization

Detailed mineralogical and micro-textural studies were undertaken at the University of Huelva (Spain). Fourteen polished thin sections from the main lithologies were studied by both petrographic microscope and scanning electron microscope coupled with energy dispersive spectroscopy (SEM–EDS) Fei-QUANTA 200 equipped with a microanalyzer EDAX Genesis 2000. Ten thin sections containing carbonates, silicates, phosphates, oxides and sulphides were selected for electron microprobe analyses (EPMA). The chemical compositions were determined using a JEOL JXA-8200 Super Probe Electron Probe Micro-Analyzer. The measurements were performed on carbon-coated polished sections using an acceleration voltage of 20 kV, 20 nA beam current, 30 s counting time for the peak and 10 s for the background. The analysis spots were selected using backscattered electron (BSE) images. Concentrations of FeO, CaO, MgO, MnO_2, SrO, BaO, CuO, ZnO, PbO, TiO_2, CuO and ZnO in carbonates and Fe-oxyhydroxides, as well as Ag, Sb, Mn, Cd, Bi, As, Sn, Co, Se, Ni, Au, Cu, Zn, Fe, Pb, Hg and S elements in sulphides and sulfosalts were determined by wavelength-dispersive spectroscopy (WDS). Up to 73 successful EPMA analyses on phosphates, 19 on carbonates, 12 on oxides and 29 on silicates have been obtained. Routine data reductions, including full matrix (ZAF) corrections, were performed. In addition, in order to perform semiquantitative mineralogical analyses on waste rock dump samples, 14 samples were

investigated by X-ray diffraction (XRD) using a Broker D8 Advance Powder Diffractometer with Cu–Kα radiation.

The mineralogy and textures of tailings were also investigated on ten polished sections by both petrographic microscope and SEM-EDS JEOL JMS-5410 equipped with a Link Oxford microanalyzer from the University College Dublin. Compositional mapping of SEM was undertaken by silicon drift detector (SDD), followed by semiquantitative mineralogical analyses by ImageJ software (https://imagej.nih.gov/ij).

3.3. Mineral dissolution by sequential extraction assays and chemical analysis

Samples were submitted to a REE leachability assay based in a sequential extraction procedure (described in appendix 2) designed to contact the residues with different chemical reagents to release the elements hosted on the different mineral phases. The selection of the following four fractions of the sequential extraction is based on the main mineralogy of these mine residues (i.e. phosphates, carbonates, Fe-oxides, sulphides and silicates); fraction 1 (F1) induces dissolution of water/acid soluble minerals and release of exchangeable elements by the use of 0.11 mol/l acetic acid, fraction 2 (F2) attacks the reducible fraction by the use of 0.1 mol/l hydroxylamine hydrochloride, fraction 3 (F3) tackled the oxidizable fraction by the use of 8.8 mol/l H_2O_2, temperature (85ºC) and 1.0 mol/l ammonium acetate and fraction 4 (F4) digests the residual fraction by the use of aqua regia (a mixture of 12 mol/l HCl and 15.8 mol/l HNO3 in the ratio 3:1) at 100ºC.

Additionally, sub-samples of all the studied residues were independently submitted to an aqua regia digestion to obtain the pseudo total bulk chemistry of the samples. Specific details about the sequential extraction procedure are offered in the Supplementary Information. The extractants of the sequential extractions were analysed at the University of the Free State by Inductively Coupled Plasma Mass Spectrometry (ICP-MS) PerkinElmer NexIon 2000c, inductively coupled plasma optical emission spectroscopy (ICP-OES) Teledyneleemanlabs Prodigy and High-Performance Liquid Chromatography (HPLC) Shimadzu prominence (analytical details in appendix 3). In addition, 20 subsamples were also analysed by an accredited laboratory at the Institute for Groundwater Studies at the University of Free Sate in order to validate the results.

4. Results and discussion

4.1. Waste rock dumps

Rock fragments of diverse lithologies were observed unevenly distributed, regarding size and mineralogical composition, along all the main slopes of the WRDs. Most common fragments include (Figure 1 and 2):

T-carbonatite is mainly comprised of calcite, magnetite, dolomite, enstatite and fluorapatite. The subordinated mineralogy consists of variable amounts of phlogopite, muscovite, chalcopyrite, bornite, chalcocite, pyrite, monazite, zircon, rutile, bastnäsite-(Ce) and anzaite-(Ce). The T-carbonatite shows phaneritic texture characterized by coarse magnetite associated with euhedral aggregates of calcite and dolomite and Cu-sulphides filling interstices (Figure 2a).

B-carbonatite is mostly composed of calcite, dolomite, magnetite, enstatite, fluorapatite and phlogopite. The minor mineralogy consisted of chalcopyrite, chalcocite, pyrite, pentlandite, olivine, serpentine, chlorite and parisite. These minerals have been observed distributed in inequigranular, euhedral to subhedral aggregates forming mm-to-cm rhythmic banding (Figure 2b).

Phoscorite is mostly formed of fluorapatite and phlogopite, and minor magnetite, ilmenite, ulvospinel, olivine, serpentine, calcite, dolomite and bornite. These minerals show phaneritic textures characterized by inequigranular euhedral fluorapatite aggregates with phlogopite and calcite filling open spaces (Figure 2c).

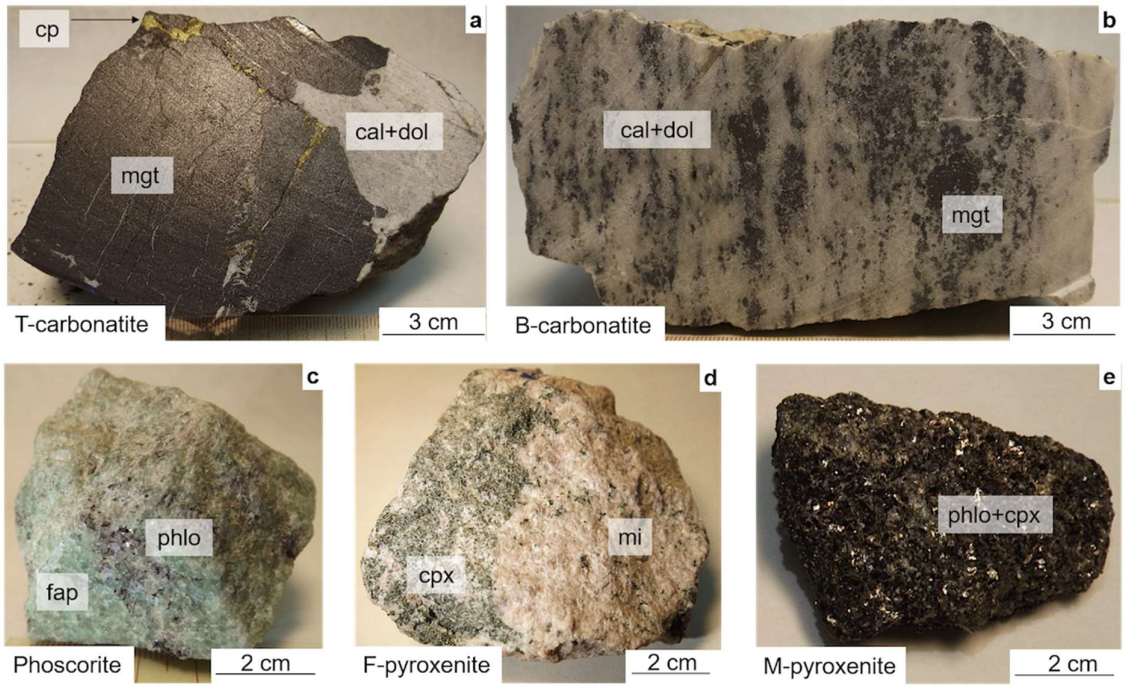

Figure 2. Rocks fragment from the waste rock dumps of Phalaborwa Igneous Complex; B-carbonatite formed of alternating band of magnetite (mgt) and calcite (cal) associated with dolomite (dol); (b) T-carbonatite composed by magnetite, calcite, dolomite and chalcopyrite (cp) filling fractures; (c) phoscorite comprised of fluorapatite (fap) associated with phlogopite (phlo); d) F-pyroxenite formed by microcline (mi) and clinopyroxene (cpx); and e) M-pyroxenite composed by phlogopite and clinopyroxene.

F-pyroxenite is mainly comprised of microcline, diopside, hydroxyapatite, fluorapatite, and subordinated amounts of calcite, magnetite, chalcopyrite, bornite and allanite. Clinopyroxenes and feldspars appear as coarse euhedral aggregates, including pegmatoid texture, whereas apatite group minerals have been observed as fine-grained euhedral to subhedral aggregates (Figure 2d).

M-pyroxenite is mainly composed of fine-grained diopside and phlogopite. The subordinated mineralogy consists of variable proportions of interstitial microcline, magnetite, hydroxyapatite, thorite and baddeleyite (Figure 2e).

4.2. Mineralogical analysis of the waste rock dumps

4.2.1. Phosphates

Several minerals from the apatite group have been identified as a major component in all the WRDs (Figure 1). Fluorapatite have been recognized in both carbonatites (Figure 3a and h) and phoscorites (Figure 3b), whereas hydroxyapatite is most common in pyroxenite fragments (Figure 3c and e).

Fluorapatites and hydroxyapatites occur as euhedral to anhedral aggregates showing a wide range of grain sizes, between a few μm to 2 mm in both carbonatites (Figure 3a and h) and pyroxenites (Figure 3c and e), and up to 4 mm in phoscorites (Figure 2c). Both hydroxyapatite and fluorapatite have been observed associated mainly with carbonates (Figure 3a), micas (Figure 3b), pyroxenes and feldspars in all the waste rock samples (Figure 3c and d).

Fluorapatite from both carbonatites and phoscorites shows similar high REE contents (mean values of 1.03 and 0.93 wt% respectively), being relatively enriched in LREE (mean values of 0.83 and 0.66 wt%, respectively) (Figure 4a). Fluorapatite grains from both carbonatites and phoscorites exhibit internal heterogeneous composition related to its REE distribution. Fluorapatite from carbonatites shows an enrichment in REE at the crystal boundaries (Figure 3a), whereas fluorapatite from phoscorites exhibits an opposite REE distribution (Figure 3b).

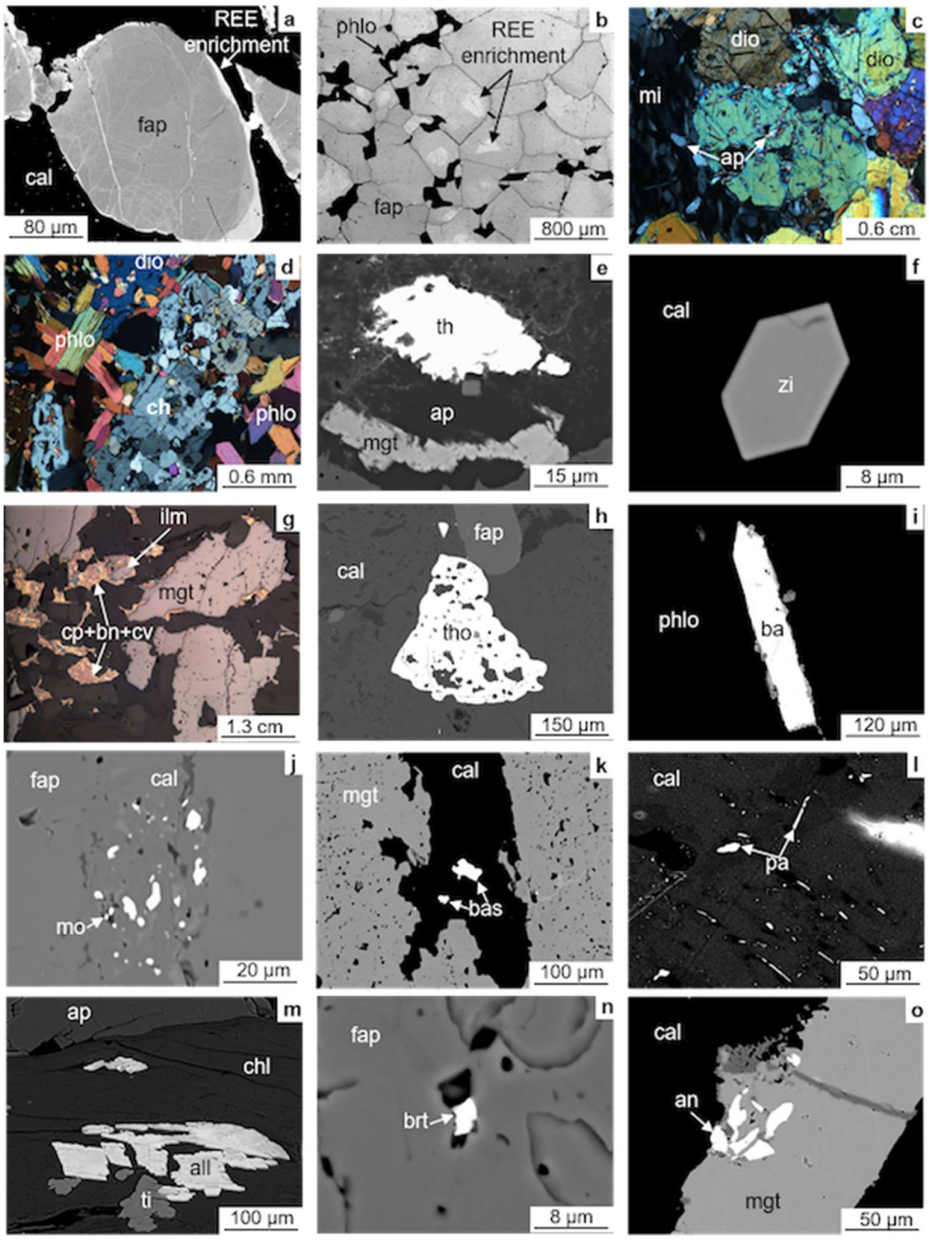

Figure 3. Reflected light and backscattered electron (BSE) images of the waste rocks; a) LREE enrichment along grain boundaries of subhedral fluorapatite (fap) included in calcite (cal); b) phlogopite (phlo) filling interstices in fluorapatite aggregate with LREE enrichment in the core grains; c) diopside (dio) aggregate with apatite (ap) inclusions and microcline (mi) filling open spaces; (d) phlogopite aggregate associated with chloritoid (ch) and diopside; e) thorite (th) filling spaces in apatite and magnetite (mgt); f) euhedral zircon (zi) grain included in calcite; g) chalcopyrite (cp), bornite (bn) and covellite (cv) filling open space in magnetite, ilmenite (ilm) and calcite crystals; h) thorianite (tho) replacing calcite; i) acicular baddeleyite (ba) crystal filling interstices in phlogopite; j) monazite (mo) inclusions in fluorapatite; (k) bastnäsite (bat) grains in calcite; (l) parasite (pa) crystals associated with calcite; (m) allanite (all) interbedded with chlorite (chl); (n) britholite (bt) inclusions in fluorapatite; (o) anzaite (an) included in magnetite.

4.2.2. Carbonates

Calcite and dolomite have been identified in all the WRDs (Figure 2a, b, Figure 3a, g, h, k, l and o). They are most abundant in carbonatites with a 3:1 ratio. These minerals occur with large variability of textures, such as coarse calcite and dolomite groundmasses in transgressive carbonatites (Figure 2b), alternating mm-to-cm bands in banded carbonatites (Figure 2a), calcite with dolomite inclusions disseminated in banded carbonatites (Figure 2a) and fine interstitial infilling in phoscorites and pyroxenites. Calcite exhibits higher REE contents than dolomite, showing mean values of 0.52 and 0.22 wt%, respectively. Both carbonates are relatively enriched in LREE (mean values of 0.35 and 0.13 wt%, respectively) (Figure 4b).

4.2.3. Silicates

Pyroxenes have been found widely distributed throughout the WRDs (Figure 2d, e, 3c and d). In carbonatites and phoscorites, enstatite has been recognized as the most common orthopyroxene, whereas in pyroxenites, diopside is the most abundant clinopyroxene. Enstatite occurs as subhedral aggregates between a 2 μm to 2 mm. Diopside appear as euhedral aggregates which is usually replaced by chlorite and showing a wide range of grain sizes, up to 10 cm (Figure 2d, e, 3c and d).

Diopside from F- and M-pyroxenites show similar low REE contents (mean values of 0.05 and 0.06 wt%, respectively), being both slightly enriched in HREE (both mean values of 0.03 wt%) (Figure 4c).

Phlogopite is the most common mica. It is broadly distributed (Figure 2c, e, and 3d) but particularly abundant in M-pyroxenites (Figure 2e and 3d). This is mainly associated with calcite, fluorapatite and magnetite in carbonatites and phoscorites (Figure 2c and 3b), whereas in pyroxenites, phlogopite is linked to diopside and microcline (Figure 2d). Phlogopite shows a wide range of textures and grain sizes, including coarse euhedral aggregates forming mica-pyroxenites (Figure 2e); fine aggregates filling interstices in fluorapatite and calcite in both phoscorites and carbonatites (Figure 3b).

Microcline has been recognized as the most common feldspar, unevenly distributed throughout WRDs and linked mostly to M-pyroxenites (Figure 1d). Microcline was observed as subhedral aggregates, up to 1 cm, associated mostly with diopside and hydroxyapatite (Figure 2d and 3c).

Thorite has been recognized as a minor mineral in both M-pyroxenite and T-carbonatite rocks fragments. Thorite has been mainly identified as micrometric inclusions in hydroxyapatite and

associated with thorianite and magnetite (Figure 3e). Based on SEM-EDAX analyses, thorite shows a high REE homogeneous composition (mean value of 3.9 wt%), being relatively enriched in LREE and MREE (mean values of 2.5 and 1 wt% respectively).

Zircon is a minor but common silicate found in all the waste rock samples. It occurs as <10 μm euhedral crystals associated with pyroxenes, carbonates and hydroxyapatite (Figure 3f). Based on SEM-EDAX analyses, zircons show a homogeneous high REE distribution, with mean values of 6 wt%.

4.2.4. Oxides

Magnetite is the most common oxide in all the waste rocks samples but mainly linked to both B- and T-carbonatite (Figure 2a, b and 3g). Magnetite shows a wide range of textures, grain sizes and an intricate relationship with other minerals. Overall, magnetite shows textures such as infilling of fractures, skeletal crystals included in pyroxenes and coarse aggregates (Figure 3e and g). Magnetite is closely associated with ilmenite and ulvospinel, showing exsolutions and intergrowth textures (Figure 3g). Moreover, magnetite is linked to the Cu-sulphides suite, showing textures such as Cu-sulphides replacing and filling interstices in magnetite aggregates (Figure 3g).

Both magnetite and ilmenite in T-carbonatite present a slightly high REE concentration (REE mean values of 0.07 and 0.06 wt%, respectively). Magnetite is relatively enriched in LREE and HREE and depleted in MREE, whereas ilmenite is enriched in HREE and MREE (Figure 4d and Appendix 4).

Thorianite has been identified as a minor but common oxide in T-carbonatite. It appears as micrometric grains associated systematically with magnetite, and to a lesser extent, with thorite (Figure 3h). Based on SEM-EDAX analyses, thorianite shows a homogeneous high REE distribution, with mean values of 10 wt%.

Baddeleyite occurs as a rare mineral in M-pyroxenite. It has been observed as 400 μm euhedral crystals embedded in phlogopite (Figure 3i). Baddeleyite SEM analyses reveal low REE concentration (mean value of 0.6 wt%).

4.2.5. Sulphides

Chalcopyrite, bornite, covellite, chalcocite, pyrite and millerite are common phases along WRDs, but mainly linked to carbonatite fragments (Figure 2a and b). These are in close relationship with magnetite (Figure 2b and 3g), and show complex textural features such as intergrowth, exsolutions, replacements and veinlets (Figure 3g).

4.2.6. REE minerals

Monazite is the most common REE. It is widely distributed throughout all the waste rocks, but linked mostly to both transgressive and banded carbonatites (Figure 4a and b). It has been observed as fine euhedral aggregates (1 to 50 μm in thickness) included in fluorapatite and calcite (Figure 3j). Monazite shows higher REE content in B-carbonatites than in T-carbonatite (mean values of 60.7 and 47.9 wt%, respectively), being both relatively enriched in LREE (mean values of 56.4 and 44.3 wt%, respectively) (Figure 4e).

Bastnäsite-(Ce,La) has been identified in T-carbonatites. It occurs mostly as 5-50 μm anhedral grains embedded in late calcite veins (Figure 3k). Ce-bastnäsite in T-carbonatite exhibits a mean REE values of 70.3, of which 62.0 wt% are LREE (Figure 4e).

Parisite has been only recognized in T-carbonatite. It occurs as elongated 1-20 μm crystals included in calcite (Figure 3l). Parisite exhibits a homogeneous REE compositions, with mean values of 53.6 wt% and enrichment in LREE up to 49.5 wt % (Figure 4e).

Allanite-(Ce) has been recognized in F-pyroxenites as 5-250 μm grains associated with titanite and included in chlorite (Figure 3m). It shows a mean REE concentration of 21.0 wt%, being relatively enriched in LREE (mean value of 18.2 wt%) (Figure 4e).

Britholite-(Ce) is mainly present in both F-pyroxenite and T-carbonatite. It has been observed as >40 μm crystals filling interstices in chlorites within pyroxenites, whereas in carbonatites occurs as 5 μm inclusions in fluorapatite (Figure 3n). It has a mean REE content of 38 wt% and enrichment in LREE up to 36 wt%.

Anzaite-(Ce) has been recognized in T-carbonatite. It appears as < 120 μm sized grains replaced by magnetite and ilmenite (Figure 3o). It shows mean REE contents of 52.3 wt %, being enriched in LREE (mean values of 40.6 wt%) (Figure 4e).

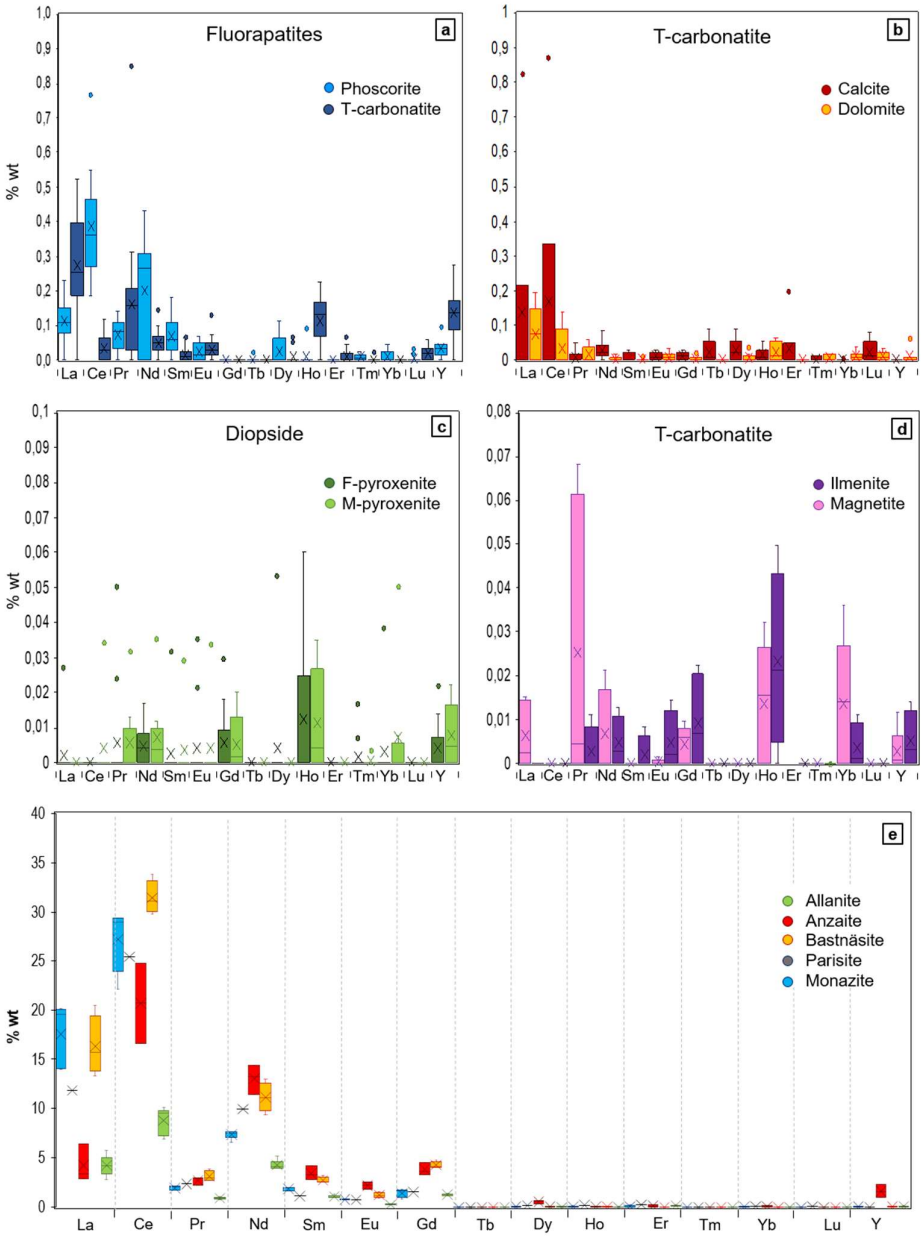

Figure 4. Rare earth elements distribution in both REE-bearing minerals and REE-minerals in waste rock dumps based on electron microprobe analyses (EPMA) analyses; a) Fluorapatite from phoscorites and T-carbonatite; b) Calcite and dolomite from T-carbonatite; c) Diopside from F-pyroxenite and M-pyroxenite; d) Ilmenite and magnetite from T-carbonatite; and e) REE content in allanite, anzaite, bastnäsite, parasite, monazite both phoscorites and T-carbonatite rocks. Extended data included in Appendix 4.

4.3. Mineralogy of tailing ponds

4.3.1. East Tailing

The main mineralogy is formed by calcite, dolomite, orthopyroxene, fluorapatite, magnetite, phlogopite, clinopyroxene and zircon. The minor mineralogy consists of chalcopyrite, ilmenite, pyrite, monazite, covellite, bornite, millerite, thorianite, ulvospinel and newly-formed Cu-sulphates (Figure 5a to e). In general terms, the mineralogy throughout East Tailing shows a homogeneous distribution, except for zircon that has only been recognized as a major component in the easternmost area (Figure 6).

Approximately, 90% of these minerals occur as monomineralic fragments, ranging from a few microns to 3 mm in diameter, most of them from 200 to 500 microns (Figure 5a and b). Some minor polymineralic fragments have been identified (Figure 5c, d and e), for example dolomite inclusions in calcite; fluorapatite and forsterite intergrowths; magnetite and ilmenite aggregates among phlogopite; micron-sized monazite inclusions in fluorapatite; and chalcopyrite associated with bornite and covellite, partially replaced by newly formed Cu-sulphate.

Monazite was a minor but common REE mineral showing a mean LREE value of 55.3 wt%. REE-bearing minerals identified in East Tailing are fluorapatite, zircon and thorianite (Figure 5). Fluorapatite has been recognized as the main REE-bearing mineral. Based on SEM-EDS analyses, most fluorapatite crystals show an enrichment in LREE in its grain boundaries reaching up to 5 wt% (Figure 5c). Zircon and thorianite-bearing REE have been punctually recognized showing a LREE concentration up to 13.2 and 10.2 wt% respectively.

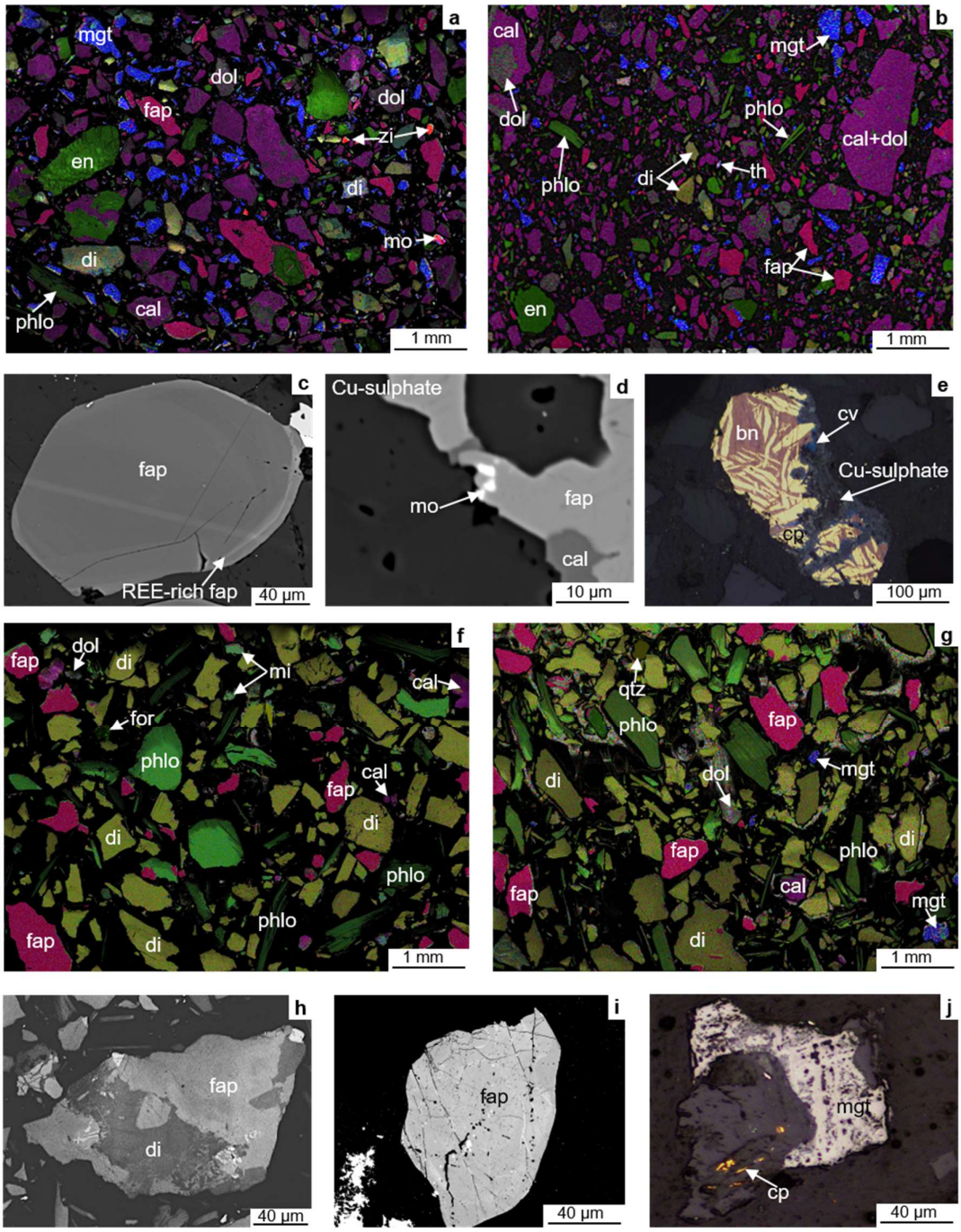

Figure 5. False-colour compositional scanning electron microscope (SEM) maps, petrographic microscope and backscattered electron (BSE) images of tailings samples; (a) and (b) Compositional SEM maps from East tailing showing the major mineralogy, including calcite (cal), dolomite (dol), enstatite (en), fluorapatite (fap), diopside (di), phlogopite (phl), magnetite (mgt), zircon (zi) and monazite (mo); (c) fluorapatite showing a REE enrichment along grain boundaries; (d) monazite inclusions in fluorapatite; e) mixed-fragment formed by chalcopyrite (cp), bornite (bn), covellite (cv) and newly-formed Cu-sulphate; (f) and (g) compositional SEM maps from Selati tailing showing the major mineralogy, such as calcite, dolomite,

fluorapatite, diopside, phlogopite, magnetite, microcline (mi) and quartz (qtz); (h) mixed fragment composed by diopside and fluorapatite; (i) subhedral fluorapatite included in calcite; (j) chalcopyrite and magnetite filling open spaces in calcite.

4.3.2. Selati Tailing

The Selati tailing is mostly comprised of phlogopite, orthopyroxene, fluorapatite, calcite, quartz, dolomite, magnetite and microcline. These minerals show a homogenous distribution throughout the tailing. The subordinated mineralogy consists of variable amounts of chalcopyrite, ilmenite, hematite, pyrite and forsterite (Figure 5f to j), although quartz and magnetite have only been identified as a major phase in the southern area and forsterite in the northern (Figure 6).

In general terms, the minerals forming the tailing show a high liberation grade (∼95%). These mainly occur as monomineralic fragments, from a few μm to 2 mm, most of them being between 300 and 800 μm (Figure 5f and g). Some minor polymineralic fragments have been identified (Figure 5h, I, and j), for example ilmenite inclusions in magnetite; fluorapatite associa ted with enstatite; intergrowths between dolomite and calcite; and chalcopyrite and magnetite filling open spaces in calcite.

Fluorapatite is the only REE-bearing mineral identified in the Selati tailing. Based on SEM-EDS analyses, fluorapatite exhibits an uneven REE distribution reaching up 10 wt% ∑LREE (Figure 5i).

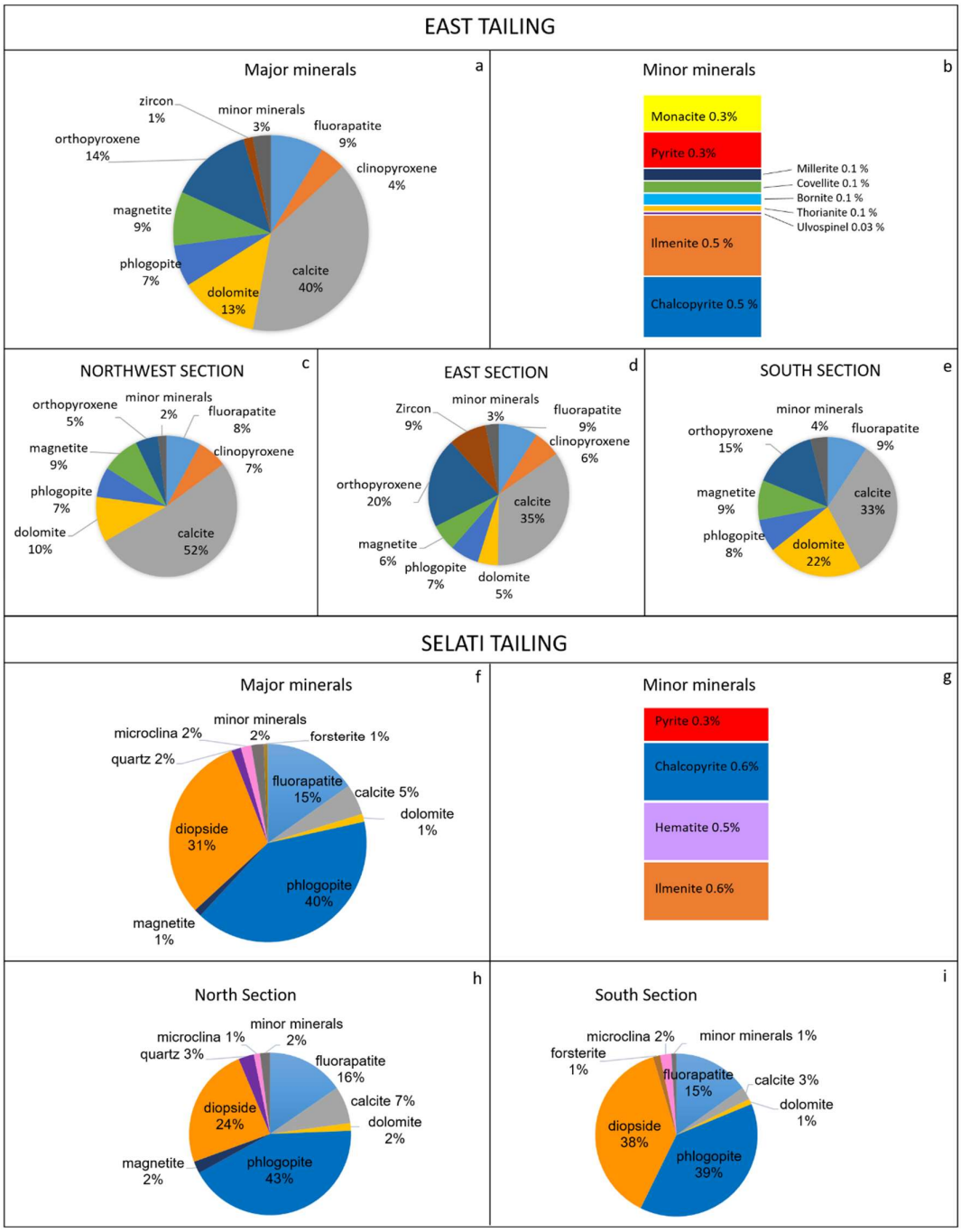

Figure 6. Mineralogical semi-quantification based on image analysis of scanning electron microscope (SEM) compositional maps of the East tailing; (a) major minerals, (b) minor minerals, (c) major minerals of northwest section, (d) of east section, (e) of south section; and the Selati tailing (f) major minerals, (g) minor minerals, (h) major minerals of north section and (i) south section.

4.4. REE sequential extraction tests

The sequential extraction efficiency, for the WRD and tailing composites, was calculated by weighting the samples before and after the extraction procedure (before F1 and after F4),

obtaining the following results: B-carbonatite, T-carbonatite, phoscorite, F-pyroxenite, M-pyroxenite, East tailing and Selati tailing were dissolved in 98.2, 99.9, 9.8, 45.5, 42.6, 89.1 and 27.0 wt%, respectively.

4.4.1. Carbonatites

Both T- and B- carbonatites showed a similar sequential dissolution behaviour (Figure 7). As previously mentioned, these two types of rocks are mainly comprised by carbonates (i.e. calcite and dolomite), magnetite, apatite and minor amounts of Cu sulphides. This mineralogical composition corresponded with the main elements released by the pseudo total (PT) digestion of both rocks (PT columns on Figure 7 and appendix 5) since Ca>Fe>Mg>P>S>Cu. However, it is important to notice, that the dissolution of the carbonates (marked by the release of Ca and Mg) was not restricted to the first digestion step (F1), it also occurred at F2, F3 and to a less extent at F4, whereas the dissolution of magnetite did not happen during F2 and took place at F4. The former behavior can be attributed to an oversaturation of the extractant respect to calcite and the concomitant impossibility to keep on dissolving more carbonates, whereas the latter is due to the inability of the reagent used to dissolve highly crystalline Fe minerals like magnetite (Caraballo et al., 2018).

T-carbonatites and B-carbonatites have ∑REE average extracted contents of 0.12 and 0.15 wt%, respectively (Figure 7b and appendix 6). Some differences can be observed on the REE release patterns for both types of carbonatites. Despite the progressive dissolution of carbonates from F1 to F3 in T-carbonatites, REE showed a tendency to remain in the mineral phases until F3; whereas REE release from B-carbonatites tends to remain in the mineral phase even further and they are mostly extracted in F4.

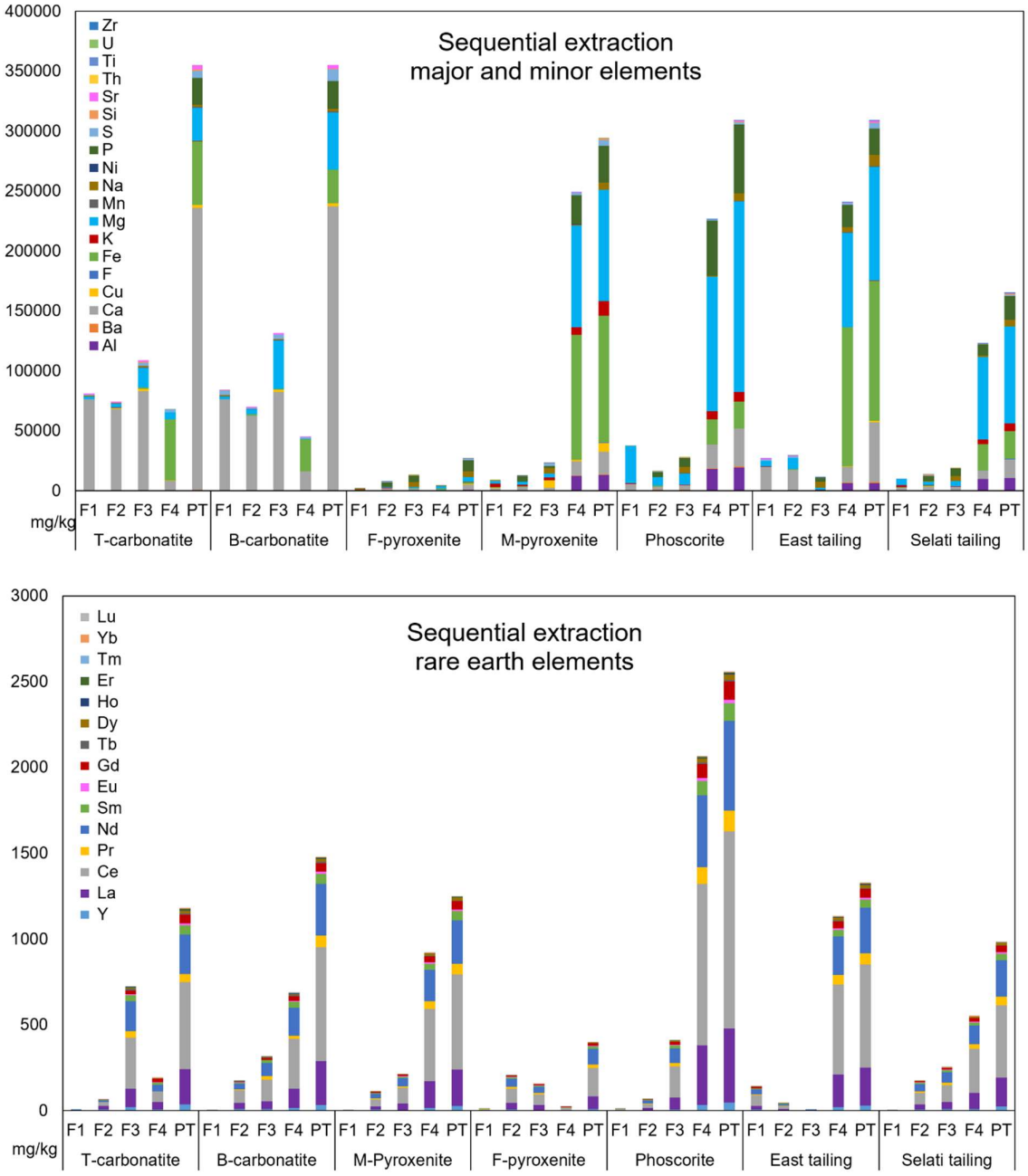

Figure 7. Elemental distribution of PIC's main lithologies and tailings in each step of the sequential extractions (F1, F2 F3 and F4) and the pseudo-total concentration in the aqua regia digestion (PT).

4.4.2. Phoscorites

As previously shown, this type of residue is mainly composed by fluorapatite and phlogopite. A small fraction of the fluorapatite (shown by P and Ca concentrations) was dissolved during F2 and F3 (Figure 7 and appendix 5), while phlogopite (marked by Mg, K and Al) was poorly

dissolved during F1, F2 and F3. The dissolution of spinel mineral group and forsterite contributes with the high concentration of Mg. The vast majority of the sample was dissolved during the aqua regia digestion (F4), including most of the fluorapatite, phlogopite and forsterite. Despite this poor dissolution efficiency (42.6%), the phoscorite is the most REE enriched lithology (0.23 wt% on average, appendix 6). Higher ∑REE concentrations might be anticipated if/when a complete sample dissolution is achieved. Ce, Nd and La were the most abundant REE released (1150, 524.1 and 430.7 mg/kg, respectively).

4.4.3. Pyroxenites

F- and M-pyroxenite show different mineral contents, with the former characterized by the presence of microcline, diopside, hydroxyapatite and the latter mainly comprised by diopside and phlogopite. As a result, they show different behaviors when underwent to the sequential dissolution protocol. F-pyroxenite only showed some dissolution of the hydroxyapatites, marked by P and Ca release, in F3 or PT (Appendix 5), whereas all other mineral phases were not disassociated. As a result of these poor dissolution, almost no discernible ∑REE was released (Figure 7 and Appendix 6). The dissolution of M-pyroxenite was mostly restricted to the aqua regia steps (F4 and PT). The low solubility of the minerals comprising this residue induced a low ∑REE recovery. Nevertheless, concentrations as high as 0.11 wt% of ∑REE were observed (Appendix 6).

4.4.4. East tailing

This residue was comprised mainly by carbonates, enstatite, magnetite, phlogopite and diopside. Some carbonates were dissolved during F1 and F2 (marked by Ca release in Figure 7 and Appendix 5) but most minerals were not dissolved until the aqua regia digestion (F4). The ∑REE recovery showed similar behavior to the release of the major element, the main recovery took place during the aqua regia digestion. An average concentration of 0.14 wt% was achieved, where Ce, Nd and La were the most abundant REEs (602.3, 266.2 and 221.5 mg/kg, respectively) (Figure 7 and Appendix 6).

4.4.5. Selati tailing

A poor dissolution efficiency (27.0 wt%) was achieved for this residue. This could be anticipated from its original mineralogy, comprised mainly by phlogopite, diopside and fluorapatite, all minerals with low solubility. As a result, most of the mineral dissolution was limited to the aqua regia extractions (F4 and PT). The concentration of ∑REE was 0.1 wt% on average, showing some progressive release from F2 to F4, with its maximum recovery in F4 (Figure 7 and Appendix 6).

4.5. REE potential of WRDs

Phosphate minerals, such as monazite and fluorapatite included in both carbonatites and phoscorite fragments, could be considered as the most interesting REE-source in PIC WRDs due to its abundance and remarkable REE concentration (Figure 3a, b, c, e, h, j, m, n; 4a and e). In this regard, monazite is the most common REE mineral in carbonatites. Fluorapatite in carbonatites has higher REE concentration than fluorapatite in phoscorite (Figure 4a), however, fluorapatite is less abundant in carbonatites (7-35 wt%) than in phoscorites (70 wt%) (Giebel et al., 2017; Milani et al., 2017; Vielreicher et al., 2000). The association of phosphate minerals and REE concentrations was demonstrated by merging mineralogical analyses with the elemental composition obtain after sequential extraction protocol implemented; EPMA results of monazite and fluorapatite show a REE concentration of 64 and 1 wt%, respectively (Figure 4a and e); while 87% of P were released during F4 —the digestion of phosphate minerals in F4 by the reaction with HCl has been previously reported (Ruttenberg, 1992)— together with 89% of REE, in phoscorite samples. Common carbonates forming the PIC WRDs may also be considered as a REE source owing to both its high abundance and its REE concentration (mean ∑REE of 0.5 wt% in calcite and 0.2 wt% in dolomite) (Figure 4b). Significantly, B-carbonatite has higher abundance of both carbonate minerals than T-carbonatite.

Minerals previously analyzed from fresh phoscorite and carbonatite samples (Dawson and Hinton, 2003; Giebel et al., 2016; Hornig-Kjarsgaard, 1998) presented lower concentration of REE than those analyzed herein from WRD fragments. For example, REE on fluorapatite, calcite and dolomite were reported in ranges of 0.5-3.9, 0.03-0.17 and 0.04-0.07 wt%, respectively, while in this study, WRD samples reach up to 4.8, 2.9 and 0.8 wt%, respectively (Appendix 4). The lower REE contents of in-situ outcrop samples can be related to magmatic differentiation processes. According to Giebel et al. (2017), most REE minerals, fluorapatite, calcite and dolomite crystalized during either orto- or late-magmatic stages in phoscorite and carbonatites. However, Cu is mostly found in the PIC core which was affected by a high sulfidation stage. Therefore, the selective extraction of Cu-rich rocks might have left relatively REE enriched rock fragments in WRDs.

Diopside is the most abundant REE-bearing mineral in both M- and F-pyroxenites from WRDs (Figure 2c, d and 3d). Heinrich (1970) described the PIC fresh pyroxenites with diopside content up to 61%. Based on EPMA analyses, diopside REE concentration from both pyroxenite types shows an average of 0.06 and maximum content of 0.3 wt%, r espectively (Figure 4c). However, diopside is quite resistant and its dissolution did not begin until the last step of the sequential digestion (F4), as shown by the digestion of phoscorite and M-

Pyroxenite samples (Figure 7 and Appendix 6). As a result, in M-pyroxenite, most REE were released in F4, also matching with high P extraction rates, probably related to monazite and hydroxyapatite dissolution (Figure 7). In contrast, most REE in F-pyroxenite were extracted in F2 and F3 associated with sulphides and oxides, such as magnetite, ilmenite and ulvospinel (with average REE concentration of 0.15 wt%), thorianite (10 wt%) and baddelayite (0.6 wt%) (Figure 3 and 7b). Taking into account that M-pyroxenite has a higher REE concentration than F-pyroxenite (average of 0.1 vs 0.05 wt%), this lithology might be considered as a secondary source of REE in PIC WRDs.

It is worth noting that resistant REE-rich minerals, such as allanite, britholite and thorite, are expected to be poorly digested during the sequential extraction. In that sense, geochemical analyses are expected to show lower REE concentration than mineralogical analyses (Appendix 4 versus 6).

4.6. REE potential of tailing ponds

Tailings can be considered as quite homogeneous anthropogenic deposits if compared with ore deposits that can show significant spatial geochemical and mineralogical changes along the multiple geological zones of the deposit. However, tailings may show some grain-size and specific-gravity driven segregations, as well as some enriched or depleted pseudo horizontal alteration fronts (Brodie et al., 1991; Chen et al., 2020; Smuda et al., 2014). Thus, a more detailed tailing sampling would enhance the reliability of the economic implications. However, they are adequate to obtain a first insight into their economic potential due to the expected homogeneity of these deposits, and to offer some light into the REE-bearing mineral phases that a possible metallurgical extraction process will have to handle.

In general terms, the tailing mineralogical composition is comparable with those identified in WRDs (Figure 6). In addition, newly-formed Cu-sulphates have been identified in the East tailing (Figure 5 and 6). Geochemical analyses showed that ∑REE of East tailing is 0.14 wt%, of which 0.11 wt% are LREE (Figure 7), while mineralogical analyses showed similar REE distribution pattern but with higher concentrations (∑REE is 0.56, of which 0.38 wt% are LREE). This pattern has been identified in fluorapatite, monazite, zircon and thorianite, from the tailing and the WRD samples, matching with the REE distribution reported for core samples from PIC (Bulakh et al., 1998; Dawson and Hinton, 2003; Giebel et al., 2019, 2017; Milani et al., 2017). Assuming that minerals from tailings would preserve the REE concentration of the original rock, the concentration of REE of the monazite in East tailing (∑REE 65 wt%) suggests that it is probably coming from the processing of mostly B-carbonatite (∑REE 61 wt%), whereas ∑REE of T-carbonatite is 48 wt% (Figure 5). Pålsson et al. (2014) also described a similar REE distribution between Fe ore deposits and their tailings.

Selati tailing also shows a homogeneous mineralogical distribution, except for quartz and magnetite (Figure 6h, i). The low abundance of calcite and dolomite (5 and 1%, respectively), together with the high abundance of phlogopite and diopside (40 and 31%, respectively), suggest that most tailing material comes from the processing of pyroxenite, particularly mica-pyroxenite, which is also pointed by the abundance of microcline (2%) (Figure 5). Fluorapatite is the major REE-bearing mineral in Selati tailing (15% abundance, Appendix 7). The scarcity of other REE-bearing minerals and REE minerals contribute to the low REE grade of this tailing (0.10 wt% according to geochemical analyses, 0.18% according to mineralogy) (Figure 6f, g, 7 and Appendix 7). Although, the proportion of LREE was also similar to the East tailing.

4.7. Waste revalorization

The lithologies of PIC present a REE abundance below the cut-off of current active mines, such as Bayan Obo, Mount Weld and Mountain Pass (Fan et al., 2016; Gambogi, 2019; Kanazawa and Kamitani, 2006; Orris and Grauch, 2002; Simandl and Paradis, 2018; Woolley, 2001). However, their WRDs are depleted in REE with respect to the ore, while PIC WRDs shows an opposite pattern. Thus, PIC tailings are also enriched in REE due to the extraction of other commodities. Nevertheless, hydrometallurgy studies to recover REE from Bayan Obo tailings are in progress (Zhang *et al.*, 2014; Zheng, Wu and Bian, 2017).

This study suggests that WRDs and tailings could have economical potential for REE. The WRDs show an average of easily extractable REO of 0.17 wt%, similar to East and Selati tailings (0.15 and 0.11 wt%, respectively, Figure 7 and Appendix 8). In both WRDs and tailings, monazite, fluorapatite and calcite are the most interesting minerals because of their high abundance and high concentration of REE (Figure 3, 4a, b, 5 and 6; Appendix 4 and 7). According to Gambogi (2019) and Orris and Grauch (2002), deposits with over 0.1 wt% REO are considered a potential REE resource (i.e., Matamula deposit, Spain, with 0.1% REO) (Vergara, 2018). In this regard, East and Selati tailings have 4.1 and 6.6 Mt of REO at 0.69 and 0.23 wt%, respectively, distributed mainly in monomineralic fragments of fluorapatite, calcite, dolomite, pyroxenes, magnetite and, in East tailing, monazite (Appendix 7). The nature of these material, REE-rich and already milled, contributes to the feasibility of its reprocessing and benefit.

Selati tailing has about 3.3 to 4.6 Mt of REO, based on sequential extraction and EPMA results, respectively (Figure 5, 6 and 7), that could be recovered from apatite group minerals at an average of 1.6 kg REO/ton (Appendix 7). In addition, East tailing has up to 1.1 kg REO/ton that could be recovered from fluorapatite, along with 3.6 kg REO/ton from calcite and dolomite via flotation (Cui, 2015) and 1.9 kg REO per ton from monazite (Appendix 7) by flotation, gravity separation, electrostatic separation and/or magnetic processes (e.g. Krishnamurthy &

Gupta, 2015). Bioleaching has also been recently explored as an alternative to recover REE from tailings (e.g. Ibrahim & El-Sheikh, 2011; Maleke et al., 2019). For instance, up to 95% recovery of REO from apatite of an Fe ore tailing has been previously reported using chemical methods (Peelman et al., 2018; Vierrether and Cornell, 1993).

Overall, beneficiation of REO from monazite, fluorapatite, calcite and dolomite, according to the mineralogical results, could generate up to 6.61 and 2.05 kg REO per ton from East and Selati tailings, respectively (Appendix 7). The monetary value of each tailing has been calculated using equation 1; taking into account the amount of waste accumulated in each tailing (m in tons), the average concentration of each REO ($\overline{x_i}$ in kg REO/t) and their individual stock value (v_i in $/kg) in February 2020. Based on the geochemical and mineralogical results, East tailing has a REO content valued between 18 and 77 billion dollars; while Selati tailing value range between 61 and 123 billion dollars. The most profitable REOs of the tailings are Nd_2O_3, Dy_2O_3, Pr_2O_3 and Tb_4O_7, which represent 87% of the net value (Appendix 8 and 9).

$$Value\ (\$) = \sum_{i=La}^{i=Y} (\overline{x_i} \cdot v_i) \cdot m \cdot 10^{-9} \qquad 1$$

The main WRD reach up to 665 Mt of rock fragments, which together with the high concentration of REE in major minerals such as fluorapatite and calcite, suggest an economic potential for REE. However, due to the heterogeneity of the WRD, a more detailed study on a comprehensive drilling campaign is recommended for a reliable feasibility study.

5. Conclusions

The study suggests that PIC possess a large volume of wastes, including waste rocks and tailings, that are enriched in REE with respect to the ore deposit. The abundance of REE minerals such as monazite (∑REE 60 wt%), and REE-bearing minerals such as fluorapatite and calcite minerals (∑REE 1 and 0.5 wt%, respectively) confirm the economic potential of PIC wastes as secondary source of REE. The most profitable REE are Nd, Dy, Pr and Tb (87% of net value). The tailings are economically more attractive than the WRDs because the mineral processing of the carbonatites and phoscorites to extract Cu and P has produced tailings of mostly monomineralic particles enriched in REE.

6. Acknowledgment

The authors thank the staff of Palabora Mining Company and Foskor for their assistance with the sampling. This research was conducted under the ERAMIN project AMDREY -PCIN2015-242-256, financially supported by the Department of Science and Technology, South Africa. It was also partially financed by: project MOS (grant number CGL2016-79204-R), which is

supported by the Spanish Government, CORFO and Codelco (project CORFO-16PTECME-66524), project CONICYT/PIA Project AFB180004, UNESCO (UNESCO-IUGS-IGCP-Project 682), Science Foundation Ireland (grant number 18/IF/6347) and SABDI/TIA project 16/1070.

7. References

Aldous, R.T.H., 1986. Copper-rich fluid inclusions in pyroxenes from the Guide copper mine, a satellite intrusion of the Palabora igneous complex, South Africa. Econ. Geol. 81, 143–155. https://doi.org/10.2113/gsecongeo.81.1.143

Basson, I., Lourens, P., Paetzold, H.D., Thomas, S., Brazier, R., Molabe, P., 2017. Structural analysis and 3D modelling of major mineralizing structures at the Phalaborwa copper deposit. Ore Geol. Rev. 83, 30–42. https://doi.org/10.1016/j.oregeorev.2016.12.002

Briden, J.C., 1976. Application of Palaeomagnetism to Proterozoic Tectonics. Philos. Trans. R. Soc. A Math. Phys. Eng. Sci. 280, 405–416. https://doi.org/10.1098/rsta.1976.0004

Brink, D., 2011. Occurrence of Groundwater in Phalaborwa Igneous Complex. University of the Free State, Bloemfontein.

Brodie, M.J., Broughton, L.M., Robertson, A.M., 1991. A Conceptual Rock Classification System For Waste Management And A Laboratory Method For ARD Prediction From Rock Piles, in: Second International Conference on the Abatement of Acidic Drainage. Vancouver, p. 17.

Bulakh, A.G., Le Bas, M.J., Wall, F., Zaitsev, A.N., 1998. Ancylite-bearing carbonatites of the Seblyavr massif, Kola Peninsula, Russia. Neues Jahrb. für Mineral. Monatshefte 171–192.

Caraballo, M.A., Serna, A., Macías, F., Pérez-López, R., Ruiz-Cánovas, C., Richter, P., Becerra-Herrera, M., 2018. Uncertainty in the measurement of toxic metals mobility in mining/mineral wastes by standardized BCR®SEP. J. Hazard. Mater. 360, 587–593. https://doi.org/10.1016/j.jhazmat.2018.08.046

Chen, T., Yan, Z.-A., Xu, D., Wang, M., Huang, J., Yan, B., Xiao, X., Ning, X., 2020. Current situation and forecast of environmental risks of a typical lead-zinc sulfide tailings impoundment based on its geochemical characteristics. J. Environ. Sci. https://doi.org/10.1016/j.jes.2020.03.010

Cui, H., 2015. Beneficiation of Rare Earth Elements Bearing Ancylite. University of Colorado.

Dawson, J.B., Hinton, R.W., 2003. Trace-element content and partitioning in calcite, dolomite

and apatite in carbonatite, Phalaborwa, South Africa. Mineral. Mag. 67, 921–930. https://doi.org/10.1180/0026461036750151

Fan, H.R., Yang, K.F., Hu, F.F., Liu, S., Wang, K.Y., 2016. The giant Bayan Obo REE-Nb-Fe deposit, China: Controversy and ore genesis. Geosci. Front. 7, 335–344. https://doi.org/10.1016/j.gsf.2015.11.005

Foskor, 2018. Foskor Intergrated Report for the Year Ended 31 March 2018. Phlaborwa.

Gambogi, J., 2019. USGS Rare earths. U.S. Geol. Surv. Miner. Commod. Summ. Febr. 2019 1, 2.

Giebel, J.R., Gauert, C.D.K., Costin, G., 2016. Rare earth minerals in the lower part of the Palabora Carbonatite Complex, South Africa. Miner. Resour. a Sustain. World. Proc. 13th SGA Bienn. Meet. 1009–1013. https://doi.org/10.13140/RG.2.1.3957.3523

Giebel, R.J., Gauert, C.D.K., Marks, M.A.W., Costin, G., Markl, G., 2017. Multi-stage formation of REE minerals in the Palabora Carbonatite Complex, South Africa. Am. Mineral. 102, 1218–1233. https://doi.org/10.2138/am-2017-6004

Giebel, R.J., Marks, M.A.W., Gauert, C.D.K., Markl, G., 2019. A model for the formation of carbonatite-phoscorite assemblages based on the compositional variations of mica and apatite from the Palabora Carbonatite Complex, South Africa. Lithos 324–325, 89–104. https://doi.org/10.1016/j.lithos.2018.10.030

Golder Associates, 2019. Draft Consolidated Environmental Management Report.

Hanekom, H.J., Van Staden, C.M.V.H., Smit, P.J., Pike, D.R., 1965. The Geology of the Palabora Igneous Complex. South African Geological Survey, Pretoria.

Heinrich, E.W.M., 1970. The Palabora carbonatitic complex - A unique copper deposit. Can. Mineral. 10, 585–598.

Hornig-Kjarsgaard, I., 1998. Rare Earth Elements in Sovitic Carbonatites and their Mineral Phases. J. Petrol. 39, 2105–2121. https://doi.org/10.1093/petroj/39.11-12.2105

Hu, L., Wu, H., Zhang, L., Zhang, P., Wen, Q., 2017. Geotechnical Properties of Mine Tailings. J. Mater. Civ. Eng. 29, 04016220-1-04016220–10. https://doi.org/10.1061/(ASCE)MT.1943-5533.0001736

Ibrahim, H.A., El-Sheikh, E.M., 2011. Bioleaching Treatment of Abu Zeneima Uraniferous Gibbsite Ore Material for Recovering U, REEs, Al and Zn. Res. J. Chem. Sci. 1, 55–66.

Kanazawa, Y., Kamitani, M., 2006. Rare earth minerals and resources in the world, in: Journal of Alloys and Compounds. https://doi.org/10.1016/j.jallcom.2005.04.033

Krishnamurthy, N., Gupta, C.K., 2015. Extractive metallurgy of rare earths, second edi. ed. CRC Press, Boca Raton.

Madugalla, T.B.N.S., Pitawala, H.M.T.G.A., Karunaratne, D.G.G.P., 2014. Use of Carbonatites in the Production of Precipitated Calcium Carbonate: A Case Study from Eppawala, Sri Lanka. Nat. Resour. Res. 23, 217–229. https://doi.org/10.1007/s11053-013-9222-8

Maleke, M., Valverde, A., Vermeulen, J.-G., Cason, E., Gomez-Arias, A., Moloantoa, K., Coetsee-Hugo, L., Swart, H., van Heerden, E., Castillo, J., 2019. Biomineralization and Bioaccumulation of Europium by a Thermophilic Metal Resistant Bacterium. Front. Microbiol. 10, 81. https://doi.org/10.3389/fmicb.2019.00081

Milani, L., Bolhar, R., Frei, D., Harlov, D.E., Samuel, V.O., 2017. Light rare earth element systematics as a tool for investigating the petrogenesis of phoscorite-carbonatite associations, as exemplified by the Phalaborwa Complex, South Africa. Min. Depos. 1105–1125. https://doi.org/10.1007/s00126-016-0708-2

Moukodi, G.P., 2008. Hydrogeochemical determination of the salt load from copper mine waste in the Bushveld Igneous Complex. University of the Free State.

Nassar, N.T., Brainard, J., Gulley, A., Manley, R., Matos, G., Lederer, G., Bird, L.R., Pineault, D., Alonso, E., Gambogi, J., Fortier, S.M., 2020. Evaluating the mineral commodity supply risk of the U.S. Manufacturing sector. Sci. Adv. 6. https://doi.org/10.1126/sciadv.aay8647

Orris, G.J., Grauch, R.I., 2002. Rare earth element mines, deposits, and occurrences. Open-File Rep. 02-189 174.

Owen, R., Madari, N., 2009. Baseline Report on The Hydrogeology of the Limpopo Basin : Country studies from Mozambique , South Africa and a contribution to the Challenge Program on Water and Food Project 17 Livelihoods : Managing risk , mitigating drought and improving water product.

Pålsson, B.I., Martinsson, O., Wanhainen, C., Fredriksson, A., 2014. Unlocking Rare Earth Elements from European apatite- iron ores. Fist Eur. Rare Earth Resour. Conf. 1, 241–251.

Peelman, S., Kooijman, D., Sietsma, J., Yang, Y., 2018. Hydrometallurgical Recovery of Rare

Earth Elements from Mine Tailings and WEEE. J. Sustain. Metall. 4, 367–377. https://doi.org/10.1007/s40831-018-0178-0

Pérez-López, R., Castillo, J., Sarmiento, A.M., Nieto, J.M., 2011. Assessment of phosphogypsum impact on the salt-marshes of the Tinto river (SW Spain): Role of natural attenuation processes. Mar. Pollut. Bull. 62, 2787–2796. https://doi.org/10.1016/j.marpolbul.2011.09.008

Ruttenberg, K.C., 1992. Development of a sequential extraction method for different forms of phosphorus in marine sediments. Limnol. Oceanogr. 37, 1460–1482. https://doi.org/10.4319/lo.1992.37.7.1460

Simandl, G.J., Paradis, S., 2018. Carbonatites: related ore deposits, resources, footprint, and exploration methods. Appl. Earth Sci. Trans. Inst. Min. Metall. 127, 123–152. https://doi.org/10.1080/25726838.2018.1516935

Smuda, J., Dold, B., Spangenberg, J.E., Friese, K., Kobek, M.R., Bustos, C.A., Pfeifer, H.R., 2014. Element cycling during the transition from alkaline to acidic environment in an active porphyry copper tailings impoundment, Chuquicamata, Chile. J. Geochemical Explor. 140. https://doi.org/10.1016/j.gexplo.2014.01.013

Stettler, E.H., De Beer, J.H., Blom, M.P., 1989. Crustal domains in the northern Kaapvaal craton as defined by magnetic lineaments. Precambrian Res. 45, 263–276. https://doi.org/10.1016/0301-9268(89)90065-X

Steyl, G., 2011. Deliverable 8 : Consolidate Phase II ESKOM-SASOL PHASE II Sustainable Salt Sinks.

Uken, R., Watkeys, M.K., 1997. An interpretation of mafic dyke swarms and their relationship with major mafic magmatic events on the Kaapvaal Craton and Limpopo Belt. South African J. Geol. 100, 341–348.

Valderrama, L., Santander, M., Paiva, M., Rubio, J., 2011. Modified-three-product column (3PC) flotation of copper-gold particles in a rougher feed and tailings. Miner. Eng. 24, 1397–1401. https://doi.org/10.1016/j.mineng.2011.05.007

Vergara, R., 2018. PRELIMINARY ECONOMIC ASSESSMENT FOR THE MATAMULAS RARE EARTHS PROJECT IN COMPLIANCE WITH THE JORC CODE. QUANTUM Min.

Verwoerd, W.J., 1993. Update on carbonatites of South Africa and Namibia. South African J. Geol. 96, 75–95.

Vielreicher, N.M., Groves, D.I., Vielreicher, R.M., 2000. The Phalaborwa (Palabora) Deposit and his Potential Connection to Iron-Oxide Copper-Gold Deposits of Olympic Damp Type, in: Porte, T.M. (Ed.), Hydrothermal Iron Ore Copper-Gold & Related Deposits: A Global Perspective. PGC Publishing, Adelaide, pp. 321–329.

Vierrether, C.W., Cornell, W.L., 1993. Rare-Earth Occurrences in the Pea Ridge Tailings. Report of Investigation 9453. US Bureau of Mines, Spokane.

Wilkin, R.T., Barnes, H.L., 1997. Formation processes of framboidal pyrite. Geochim. Cosmochim. Acta 61, 323–339. https://doi.org/10.1016/S0016-7037(96)00320-1

Woolley, A.R., 2001. Alkaline Rocks and Carbonatites of the World: Part 3 Africa. The Geological Society, London.

Wu, F.-Y., Yang, Y.-H., Li, Q.-L., Mitchell, R.H., Dawson, J.B., Brandl, G., Yuhara, M., 2011. In situ determination of U–Pb ages and Sr–Nd–Hf isotopic constraints on the petrogenesis of the Phalaborwa carbonatite Complex, South Africa. Lithos 127, 309–322. https://doi.org/10.1016/J.LITHOS.2011.09.005

Zhang, B., Liu, C., Li, C., Jiang, M., 2014. A novel approach for recovery of rare earths and niobium from Bayan Obo tailings. Miner. Eng. 65, 17–23. https://doi.org/10.1016/j.mineng.2014.04.011

ZHENG, Q., WU, W., BIAN, X., 2017. Investigations on mineralogical characteristics of rare earth minerals in Bayan Obo tailings during the roasting process. J. Rare Earths 35, 300–308. https://doi.org/10.1016/S1002-0721(17)60913-X